Enhancing phenol adsorption on $Pd/SiO_2\,$

to achieve faster and more selective hydrogenation

Jason A. Chalmers, ¹ Hyunjin Moon, ¹ Samantha F. Ausman, ¹ Cheng-Hsun Chuang, ¹ Susannah L. Scott^{1,2,*}

Abstract

The effect of catalyst hydrophobicity on the kinetics of hydrogenation of aqueous phenol was investigated. The hydrophobicity of a Pd/SBA-15 catalyst was altered by incorporating biphenylene linkers into the framework of an ordered mesoporous silica. Partitioning of phenol between the aqueous solution and the pores favors the hydrophobic catalyst by an order of magnitude at room temperature, relative to the hydrophilic catalyst. The rate of hydrogenation at 75 °C is higher in the hydrophobic catalyst, as is the selectivity for the partial hydrogenation product, cyclohexanone. Analysis of kinetic profiles measured using *operando* ¹³C NMR reveals that the hydrophobic catalyst has a larger apparent adsorption constant for phenol, which results in higher phenol surface coverage and, consequently, faster and more selective hydrogenation to cyclohexanone.

Keywords: Phenol hydrogenation, Cyclohexanone selectivity, Catalyst hydrophobicity, Microkinetic modelling

Statements and Declarations

The authors declare no competing interests.

1. Introduction

The catalytic hydrogenation of phenol has been extensively studied, in part due to its industrial importance: cyclohexanone and cyclohexanol are used to produce caprolactam (the monomer used to make nylon 6) and adipic acid (one of the monomers used to make nylon 66), respectively [1, 2]. The conventional route to phenol starts with the alkylation of benzene with propene, followed by cumene oxidation to phenol and acetone [1, 3]. However, phenol can also be

¹ Department of Chemical Engineering, University of California, Santa Barbara, California 93106, United States

² Department of Chemistry and Biochemistry, University of California, Santa Barbara, California 93106, United States

^{*}Corresponding author: Susannah Scott (<u>sscott@ucsb.edu</u>)

obtained from alternative carbon sources such as lignin [4, 5]. The prospect of renewable phenol has further increased interest in its selective hydrogenation, because cyclohexanone is potentially useful in the production of biofuels [6–10].

The catalytic reaction has also been explored due to its kinetic complexity. The rate and selectivity in phenol hydrogenation depend on several factors, including the identity of the metal catalyst, the choice of solvent, and the hydrogen source [11]. Pd-based catalysts are known to be especially selective for cyclohexanone, with some studies reporting yields over 90 % at high phenol conversions (above 85 %) [12–16]. The influence of catalyst hydrophobicity on phenol hydrogenation is of current interest. One study reported higher cyclohexanone selectivity for hydrophilic Pd/C compared to hydrophobic Pd/C [12]. Similarly, phenol hydrogenation was reported to be faster and cyclohexanone selectivity higher for a hydrophilic Pd/Al₂O₃ catalyst compared to a hydrophobic Pd/C catalyst [13]. The effect was attributed to the difference in cyclohexanone hydrogenation rates [12], however, adsorption constants and rate constants were not separately quantified. Molecular dynamics simulations predicted that hydrophilic supports increase the local concentration of phenol near the Pd active sites, thereby promoting phenol adsorption onto Pd [17]. In contrast, our recent study showed much higher adsorption of phenol (ca. 10x) from water onto a hydrophobic biphenylene-bridged periodic mesoporous organosilica (PMO), compared to a hydrophilic inorganic SBA-15 silica with a similar hydroxyl density and B.E.T. surface area [18]. This apparent contradiction inspired us to investigate further to understand how surface hydrophobicity influences phenol adsorption and selective hydrogenation to cyclohexanone.

In this study, the effects of support hydrophobicity on Pd-catalyzed phenol hydrogenation activity and selectivity were explored, while minimizing differences in other catalyst variables. Two periodic mesoporous SBA-15-type materials were synthesized with similar surface areas, pore sizes, and surface hydroxyl contents, but different surface hydrophobicities. The hydrophilic silica support, designated T, was synthesized by templated condensation of tetraethylorthosilicate (TEOS, Si(OEt)₄). The hydrophobic silica support, designated BP, was synthesized by templated condensation of a biphenylene-bridged disilane, (EtO)₃SiC₆H₄-C₆H₄-Si(OEt)₃. The biphenylene linkers incorporated into the SBA-15 framework can act as entropy hotspots for solute adsorption [18]. Each support was modified with Pd nanoparticles to obtain catalysts with similar metal loadings but different hydrophobicities.

Operando ¹³C MAS-NMR can provide high quality kinetic data for organic reactions catalyzed by solid catalysts. Signals for individual reacting molecules are readily and quantitatively detected in real time, especially when enhanced by selective ¹³C enrichment, without perturbing the system by sampling. This technique has been used to obtain high-quality kinetic information for reactions at moderately elevated temperatures and pressures, including cyclohexanol dehydration [19], glucose isomerization [20], and benzyl phenyl ether hydrogenolysis [21]. MAS NMR rotors can be considered to be well-mixed, isothermal batch reactors. The use of selectively ¹³C-labeled phenol (**Scheme 1**) facilitates the fast acquisition of spectral arrays and the extraction of kinetic profiles. The performance of two catalysts with the same Pd loading and dispersion but very different water affinities (hydrophilic Pd-T and

hydrophobic Pd-BP) was investigated in aqueous phenol hydrogenation by extracting and analyzing kinetic profiles to obtain adsorption and rate constants for each catalyst.

Scheme 1. Pd-catalyzed hydrogenation of phenol-1-¹³C, showing the locations of the isotopic label (grey ball)

$$\begin{array}{c|cccc} OH & O & OH \\ \hline & 2 H_2 & \hline & Pd & \hline \end{array}$$

2. Materials and Methods

2.1. Chemicals

Tetraethylorthosilicate (98%), 4,4′-bis(triethoxysilyl)-1,1′-biphenyl (95%), Pd(II) acetate, and acetonitrile (≥99.8%) were purchased from Sigma Aldrich. ¹³C-labeled phenol (1-¹³C, 99 % isotopic enrichment) was obtained from Cambridge Isotope Laboratories. H₂ (both 5 % in N₂, and 10 % in Ar), H₂ (UHP), and He (UHP) were purchased from Airgas. All chemicals were used asreceived.

2.2. Catalyst Preparation

The periodic mesoporous silicas T and BP were prepared by templated condensation of $Si(OEt)_4$ (TEOS) and $(EtO)_3SiC_6H_4$ - C_6H_4 - $Si(OEt)_3$, respectively, following previously described procedures [18]. Each silica (250 mg) was used to prepare a supported catalyst (Pd-T and Pd-BP) by modification with $Pd(OAc)_2$ (5.3 mg in acetonitrile) using the incipient wetness method. Each catalyst was dried at 80 °C in air for 3 h to remove the solvent, then heated in air at 1 °C/min to 300 °C and held at that temperature for 2 h to remove the ligands. Finally, the catalysts were reduced at 200 °C in flowing H_2 (5 % in N_2). They were stored in a N_2 -filled glovebox until further use. The Pd loading, measured by inductively coupled plasma (ICP) atomic emission spectroscopy, was 0.95 wt%.

2.2. Catalyst Characterization

The hydrophobicity of each material was characterized previously [18, 22]. The relative surface polarity of each dry material was estimated from the fluorescence spectrum of adsorbed Prodan, recorded using a Horiba FluoroMax 4 spectrometer. The values of λ_{max} are 509 (corresponding to a polarity slightly higher than methanol) and 473 nm (corresponding to a polarity similar to 1-octanol) for Pd-T and Pd-BP, respectively, confirming a less polar (and therefore more hydrophobic) environment for the Pd-BP surface [18].

The hydroxyl density of each catalyst support was measured by a stoichiometric reaction with VOCl₃, following a previously described procedure [18, 23]. First, physisorbed water was removed by evacuation at 170 °C and 10⁻⁴ Torr for 7 h. The dried silica (30 mg) was then treated with excess VOCl₃ vapor for 0.5 h. Chemisorbed vanadium was extracted with a solution (0.5 mL)

of H₂SO₄ (1 M) and H₂O₂ (0.26 M). The absorbance of the soluble peroxovanadium complexes was measured at 450 nm [23], using a UV-2401 spectrophotometer (Shimadzu). A calibration curve prepared using ammonium vanadate served to convert absorbance at 450 nm to vanadium concentration.

Pd dispersion was determined by CO chemisorption on a Micrometrics Autochem ii 2920, equipped with a TCD detector. One set of catalysts has a dispersion of 52 % (assuming 1 CO/Pd), corresponding to an average particle diameter of ca. 2 nm (assuming a hemispherical particle shape). A second set of catalysts has a Pd dispersion of 17 %, corresponding to an average particle diameter of ca. 5 nm. In all kinetics experiments, the total catalyst loading was adjusted to keep mol_{Pd,surface} constant, although the amount of support necessarily changed.

B.E.T. surface areas were determined from N_2 sorption isotherms on a 3 Flex Micrometrics porosimeter, assuming an area for the adsorbed N_2 molecule of 0.135 nm² [24]. The values for PdT and Pd-BP are 785 and 607 m²/g, respectively. The B.J.H. method was used to estimate the average pore diameter, using the adsorption branch of the N_2 sorption isotherm. The pore diameters of Pd-T and Pd-BP are 5.3 and 9.4 nm, respectively. Catalyst properties are summarized in **Table S1**.

The amount of phenol adsorbed at room temperature was measured by mixing 20 mg of support (or catalyst) with an aqueous solution (1.5 mL) containing 50 mM of phenol. The mixture was agitated for 2 h at 3000 rpm in an IKA Vortex 4 digital mixer, then centrifuged for 5 min at 3000 rpm and decanted to separate the solid. The decanted liquid was analyzed by solution-state ¹H NMR (Varian Unity, 500 MHz).

2.3 Reaction monitoring by operando MAS NMR spectroscopy

Phenol hydrogenation was monitored using *operando* Magic Angle Spinning (MAS) NMR spectroscopy on a Bruker Avance NMR spectrometer equipped with a 11.7 T magnet and a MAS triple resonance probe. A solid-state NMR rotor (i.d. 7.5 mm, volume 0.4 mL, Revolution NMR) [25] was loaded with 1- 13 C-phenol (6.0 mg), catalyst (3.8 - 12 mg), and Milli-Q water (120 μ L). The rotor was pressurized with H₂ (50 bar) at room temperature. After heating to 75 °C inside the probe and establishing a MAS rate of 3 kHz, recording of 13 C MAS NMR spectra commenced. The amount of liquid water vaporized was estimated with Aspen Plus V10 (Aspen Technology, Inc) to be < 1 μ L. Consequently, the initial phenol concentration was ca. 530 mM. The relative concentrations of phenol, cyclohexanone, and cyclohexanol during the reaction were estimated by integration of all signals in the regions centered near 154, 219, and 69 ppm, respectively.

NMR spectra were deconvoluted in MATLAB with nonlinear least-squares regression analysis. The spectra were fit with either one or two mixed Gaussian-Lorentzian functions. The chemical shift of the solution phase species was fixed at the same value for both catalysts. Peak areas were determined by numerical integration.

2.4 Microkinetic Modelling

A microkinetic model describing the mechanism of phenol hydrogenation was developed, using a Langmuir-Hinshelwood kinetic expression to model quasi-equilibrated adsorption/desorption on the active sites, and rate-controlling surface reactions. The change in the

concentration of each reactive species was described as a function of time using ordinary differential equations (ODEs). The system of ODEs was fitted to the kinetic data using nonlinear least-squares regression in Python to estimate adsorption constants and rate constants at the reaction temperature.

3. Results and Discussion

3.1. Qualitative effect of catalyst hydrophobicity on the rate of phenol hydrogenation

Figure 1a shows a typical NMR spectral array recorded during the hydrogenation of phenol (64 μmol, 530 mM) catalyzed by Pd-T at 75 °C. Kinetic profiles extracted from this array are shown in **Figure 1b**. Their shapes and timescales closely resemble those reported using *in situ* ATR-IR spectroscopy for aqueous phenol hydrogenation catalyzed by Pt/C at 80 °C [26]. Since our ¹³C NMR signal intensities were optimized to be quantitative, the relative intensities reflect the amount of each species present in the bulk solution, the catalyst pore solution, the surface of the silica support and, in principle, the vapor phase. Under the reaction conditions used here, phenol is observed only in solution (i.e., in the bulk solution and/or in the pores) and adsorbed on the pore walls; vaporization is negligible. Phenol adsorbed on the Pd nanoparticles was not detected; its signal is expected to be strongly perturbed by Knight-shift effects, however, it represents only a very small fraction (< 0.3 %) of the total phenol present. The total integrated NMR intensity in a typical experiment varied by less than 10 % over the course of the reaction (**Figure S1**), indicating that the mass balance is stable.

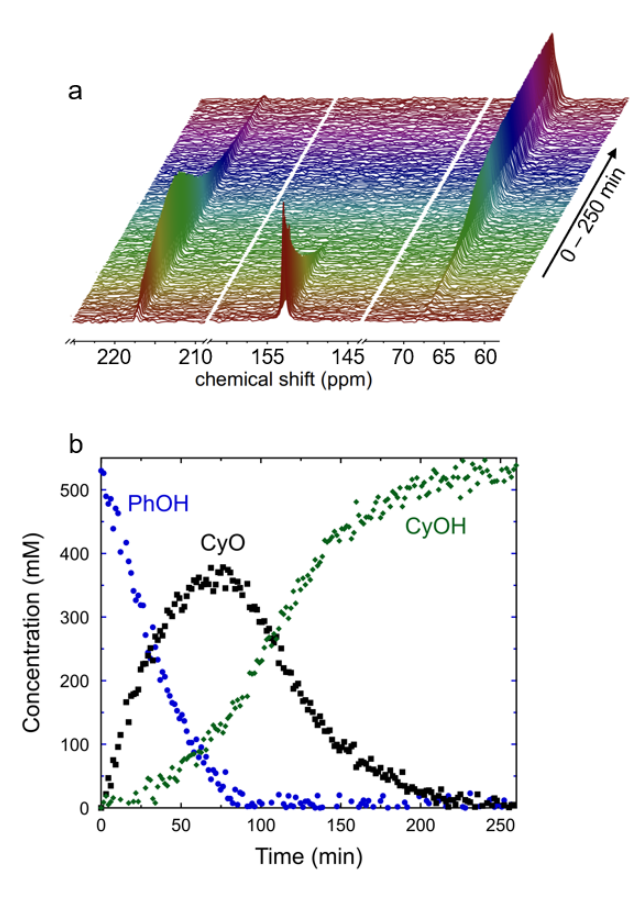


Figure 1. (a) Array of *operando* 13 C MAS-NMR spectra, showing the evolution of signals over 250 min for phenol (154 ppm), cyclohexanone (219 ppm), and cyclohexanol (69 ppm). (b) Kinetic profiles extracted from the array of 13 C MAS-NMR spectra. The MAS rotor was charged with phenol-1- 13 C (64 μmol), Pd-T catalyst (3.8 mg, 52 % Pd dispersion, 0.18 μmol surface Pd), water (120 μL), and H₂ (50 bar, 900 μmol), then heated to 75 °C. The H₂ pressure increases to ca. 60 bar at the reaction temperature.

In this experiment, phenol conversion was essentially complete after 90 min. Initially, it was converted to cyclohexanone in moderate yield (max. 375 mM, 70 % yield after 80 min). Cyclohexanone hydrogenation was slow initially but accelerated after phenol was completely converted, suggesting that phenol adsorption on the active sites blocks cyclohexanone adsorption and reaction. The hydrogenation of cyclohexanone is noticeably slower than the hydrogenation of phenol.

Under identical reaction conditions, phenol was hydrogenated noticeably faster by the hydrophobic catalyst (Pd-BP), requiring just 50 min to achieve complete phenol conversion (**Figure 2a**). In addition, the shape of the phenol profile changed from the nearly-exponential decay (i.e., approx. pseudo-first-order) observed for Pd-T to nearly linear (i.e., approx. pseudo-zerothorder) for Pd-BP. As well as being more reactive towards phenol, Pd-BP is also more selective towards cyclohexanone (max. 450 mM, 85 % yield after 50 min, **Figure 2b**). Subsequent hydrogenation of cyclohexanone to cyclohexanol is also faster over Pd-BP, and accelerates abruptly when the phenol is fully converted (**Figure 2c**). The same trends (faster rate and higher cyclohexanone selectivity for the hydrophobic catalyst) were observed with the second batch of catalysts, having lower Pd dispersion but with the same amount of surface Pd present in the reactor (**Figure S2**).

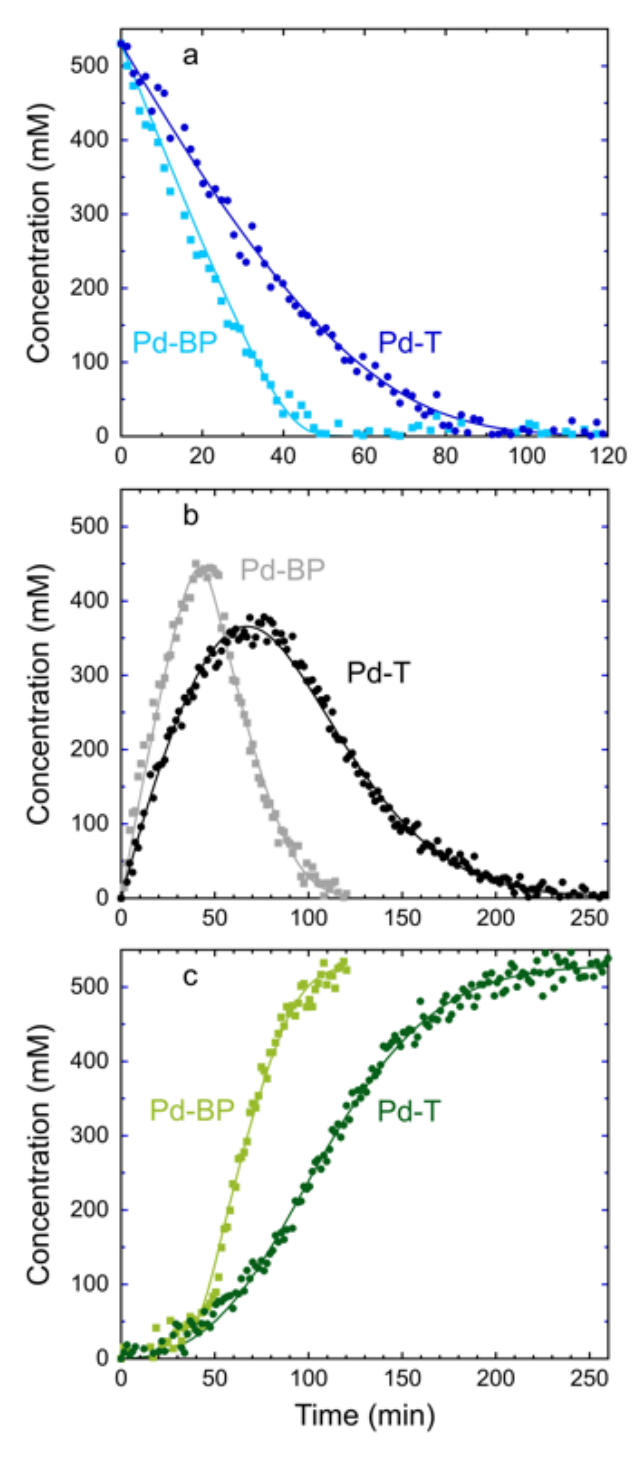


Figure 2. Comparison of kinetic profiles (points) and global curvefits (lines) for (a) hydrogenation of phenol, (b) formation and subsequent hydrogenation of cyclohexanone, and (c) formation of cyclohexanol, catalyzed by either Pd-BP or Pd-T. The MAS rotor was charged with phenol (64 μ mol), catalyst (3.8 mg, 52 % Pd dispersion, 0.18 μ mol surface Pd), water (120 μ L), and H₂ (50 bar, 900 μ mol), then heated to 75 °C. The pressure increases to ca. 60 bar at the reaction temperature. The curvefits were obtained using a Langmuir-Hinshelwood microkinetic model (see text).

3.2. Curvefitting of kinetic profiles

The kinetic profiles were analyzed using a simple microkinetic model. We assume that a single type of Pd active site (*, of unspecified ensemble size n) is available for adsorption of organics (displacement of adsorbed water is not described explicitly in the model, but is implied in the formulation of the active site as *). Phenol (PhOH) and cyclohexanone (CyO) adsorb reversibly onto the Pd sites with apparent adsorption constants K_i , eqs 1-2. Note that the adsorption constants are defined in terms of bulk solution concentrations. A step representing adsorption of cyclohexanol (CyOH) was initially included as well, but was later discarded when it turned out to be kinetically insignificant (see below). Since H_2 is present in large excess (ca. 14 mol/mol phenol), its concentration can be considered effectively constant and is not included in the site balance. Irreversible hydrogenation of phenol and cyclohexanone occurs with pseudo-first-order rate constants k_i , eq 3-4 respectively (obviously, these are not elementary reactions).

$$PhOH + * \leftrightarrows PhOH^* \qquad K_{PhOH}$$
 (1)

$$CyO + * \subseteq CyO^* \qquad K_{CyO} \qquad (2)$$

$$PhOH^* + 2 H_2 \rightarrow CyO^* \qquad k_{PhOH}$$
 (3)

$$CyO^* + H_2 \rightarrow CyOH + * \qquad k_{CvO}$$
 (4)

A system of coupled ODEs based on this microkinetic model, with four variable parameters (k_{PhOH} , k_{CyO} , k_{CyO}), was refined to each set of three kinetic profiles (see the Supplemental Information for details). The curvefits are shown superposed on the data in **Figure 2**. The model captures all of the major trends well, including the change from near-first-order phenol conversion for Pd-T to near-zeroth-order phenol conversion for Pd-BP, as well as the abrupt onset of cyclohexanone hydrogenation once phenol is nearly fully converted, and the acceleration of cyclohexanol formation and subsequent near-first-order conversion of cyclohexanone to cyclohexanol.

3.3. Quantitative effect of catalyst hydrophobicity on the kinetics of phenol hydrogenation

The best-fit values for K_i and k_i obtained from the curvefits in **Figure 2** are given in **Table 1.** The rate constants k_{PhOH} and k_{CyO} are both ca. 40 % higher for Pd-BP than for Pd-T, consistent with the higher activity observed for the hydrophobic catalyst. Unexpectedly, the latter has $k_{PhOH}/k_{CyO} = 1$ while the ratio for the hydrophilic catalyst is greater than 1, despite the finding that the hydrophobic catalyst is more selective to cyclohexanone than the hydrophilic catalyst. This finding implies that the high cyclohexanone selectivity of Pd-BP originates in differences in adsorption constants (K_i) , rather than in rate constants (k_i) .

Table 1. Comparison of fit parameters^a (adsorption constants and rate constants)^b for aqueous phenol hydrogenation^c catalyzed by Pd dispersed on a hydrophilic vs. hydrophobic support

Fit Parameter	Catalyst		
	Pd-T	Pd-BP	
$K_{PhOH}(M^{-1})$	21 (4)	140 (40)	
$K_{CyO}(\mathrm{M}^{-1})$	4.4 (1.5)	8.5 (3.3)	
K_{PhOH}/K_{CyO}	4.8 (1.8)	17 (8)	
$k_{PhOH}(s^{-1})$	0.12 (0.01)	0.16 (0.01)	
$k_{CyO}(s^{-1})$	0.098 (0.017)	0.16 (0.02)	
k_{PhOH}/k_{CyO}	1.2 (0.2)	1.0 (0.1)	

^a Obtained by curvefitting the microkinetic model (see text) to the kinetic profiles in Figure 2, to obtain least-squares estimates of the model parameter values. Values in parentheses are 95 % confidence intervals. Details and sample calculations are in the Supplementary Information.

Consistent with this hypothesis, while both catalysts have $K_{PhOH}/K_{CyO} > 1$, the difference in K_i values is larger for Pd-BP (**Table 1**). In addition, the K_{CyO} values are similar for the two catalysts, but the value of K_{PhOH} is significantly larger for Pd-BP. This difference in K_{PhOH} values is consistent with the change in shape of the phenol kinetic profiles in **Figure 2a** (i.e., closer to linear for Pd-BP, and closer to an exponential decay for Pd-T). Specifically, the larger value of K_{PhOH} for Pd-BP causes the Langmuir-Hinshelwood rate law in eq 5 (derived in the Supplementary Information) to approach the pseudo-zeroth-order limiting form in eq 6, while the smaller value of K_{PhOH} for Pd-T approaches the pseudo-first-order limiting form of the rate law in eq 7.

$$-\frac{dC_{PhOH}}{dt} = \frac{1}{V} \frac{N_{Pd}k_{PhOH}K_{PhOH}C_{PhOH}}{(1 + K_{PhOH}C_{PhOH} + K_{CyO}C_{CyO})}$$
 (5)

$$-\frac{dC_{PhOH}}{dt} \approx \frac{1}{V} N_{Pd} k_{PhOH} \tag{6}$$

$$-\frac{dC_{PhOH}}{dt} \approx \frac{1}{V} N_{Pd} k_{PhOH} K_{PhOH} C_{PhOH} \tag{7}$$

The limiting form in eq 6 requires the active sites of Pd-BP to be essentially fully occupied by phenol during the initial phase of the reaction, while eq 7 requires the active site occupancy to be much lower for Pd-T. The surface coverages θ_{PhOH} and θ_{CyO} were calculated using the model fit parameters in **Table 1** and are compared for the two catalysts in **Figure 3**. At all conversions, the phenol coverage is larger for Pd-BP than for Pd-T. The difference increases with conversion throughout the reaction, such that the coverage at 85 % conversion on Pd-BP ($\theta_{PhOH} = 0.72$) is approx. double that on Pd-T ($\theta_{PhOH} = 0.38$). At this point in the reaction, the amount of phenol remaining (ca. 10 µmol) is still much greater than the number of Pd surface sites (ca. 0.2 µmol), allowing for high coverage regardless of the ensemble requirement for phenol adsorption. As expected, the active sites of the less selective catalyst (Pd-T) adsorb more cyclohexanone compared to Pd-BP when phenol is present. However, when phenol is nearly fully consumed, Pd-

^b Adsorption constants do not account for the participation of water. Rate constants are normalized per mol surface Pd and the liquid volume under reaction conditions.

^c Reaction conditions shown in **Figure 2**.

BP adsorbs more cyclohexanone, consistent with faster hydrogenation of the intermediate (and the higher value of k_{CyO}) for the hydrophobic catalyst.

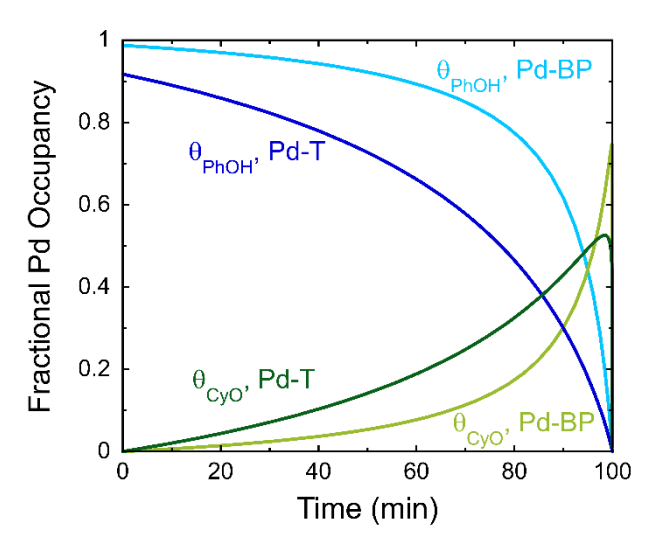


Figure 3. Fractional occupancy of the Pd_n active sites (of unspecified ensemble size n) for Pd-BP and Pd-T, by phenol and cyclohexanone in water at 75 °C in the presence of ca. 60 bar H_2 . The coverage values were calculated using the model fit parameters in **Table 1**.

As mentioned in section 3.2, the curvefits are insensitive to the inclusion of a cyclohexanol adsorption constant in the model. In particular, the root-sum squared error (RSSE) did not change when a K_{CyOH} parameter was added, **Table S2**. Thus K_{CyOH} is likely much smaller than either K_{PhOH} or K_{CyO} . This prediction is consistent with adsorption of phenol and cyclohexanone onto Pd being driven by π -interactions involving the phenol ring, or the cyclohexanone carbonyl group, neither of which is available to cyclohexanol. The adsorption of phenol on Pd(111) was computed to be driven by a combination of σ/π interactions [27].

3.4 Origin of enhanced activity and selectivity for the hydrophobic catalyst

Since the activity of a porous catalyst can be influenced by the rate of diffusion into the pores where the active sites are located, the lower activity of Pd-T compared to Pd-BP could in principle arise due to slower phenol diffusion into and/or through the hydrophilic catalyst pores, leading to a lower concentration of phenol in the Pd-T pore solution. However, the porosities of both catalysts are similar (0.24 and 0.20, respectively, **Table S1**). Their tortuosities are minimal, since ordered mesoporous SBA-15-type materials have straight and highly uniform pores [28]. In addition, the average pore diameter of Pd-T (9.4 nm) is larger than that of Pd-BP (5.3 nm, **Table S1**), therefore we expect phenol diffusion to be faster (or at least, not to be slower) in the pores of Pd-T. In fact, both mesopore diameters are much larger than the dimensions of a phenol molecule (ca. 0.6 nm [29]), making it likely that phenol experiences bulk diffusion in the pores of both materials [30]. To confirm that the phenol hydrogenation is not influenced by the rate of pore diffusion, Pd-T was sieved prior to use. Although the larger catalyst particles (425-1000 µm) are visibly different from the smaller particles (< 60 µm, **Figure S3**), their kinetic profiles for phenol consumption were indistinguishable (**Figure S4**).

Alternatively, the hydrophobic BP support may increase adsorption of phenol overall, thereby increasing the phenol coverage of active sites (see below). In our recent study of room temperature phenol sorption, we reported that the BP organosilica (i.e., without Pd) takes up nearly 10x more phenol from aqueous solutions (initial $C_{PhOH} = 10 - 70$ mM) than the inorganic T silica [18]. Comparable sorption experiments were conducted with the Pd-containing materials under the same conditions. They confirm that the presence of Pd has little effect on *overall* phenol adsorption (**Table S4**). Since the pore volumes of the two silicas are similar (**Table S1**), we assume the total amount of phenol present in the pore solutions is similar. Consequently, greater phenol sorption by the hydrophobic material implies more phenol adsorbed on the pore walls.

NMR signals for adsorbed molecules with reduced mobility are broader than for molecules moving freely in solution. *Operando* ¹³C NMR experiments were therefore conducted to quantify adsorbed phenol and cyclohexanone under reaction conditions. The catalysts with lower Pd dispersion were used for this purpose, in order to increase the ratio of support adsorption sites to Pd adsorption sites (the solid loading in the NMR rotor was adjusted to keep the number of surface Pd sites constant). For both catalysts, the ¹³C signal for solution-phase phenol appears at 154.0 ppm. At ca. 50 % phenol conversion over Pd-T, this peak is narrow and symmetrical (FWHM = 0.29 Hz) and represents 85 % of the visible phenol, **Figure 4a**. A broader peak at 154.8 ppm (FWHM = 0.44 Hz) representing 15 % of phenol present as adsorbed molecules. At the same conversion over Pd-BP, the phenol signal is broad and unsymmetrical, with a shoulder at 154.3 ppm (FWHM 0.49 Hz, **Table 3**). This shoulder represents 45 % of the phenol. Since the amount of adsorbed phenol is ca. 3x higher for Pd-BP than Pd-T (at similar phenol concentrations), Pd-BP clearly adsorbs significantly more phenol than Pd-T on its pore walls under reaction conditions.

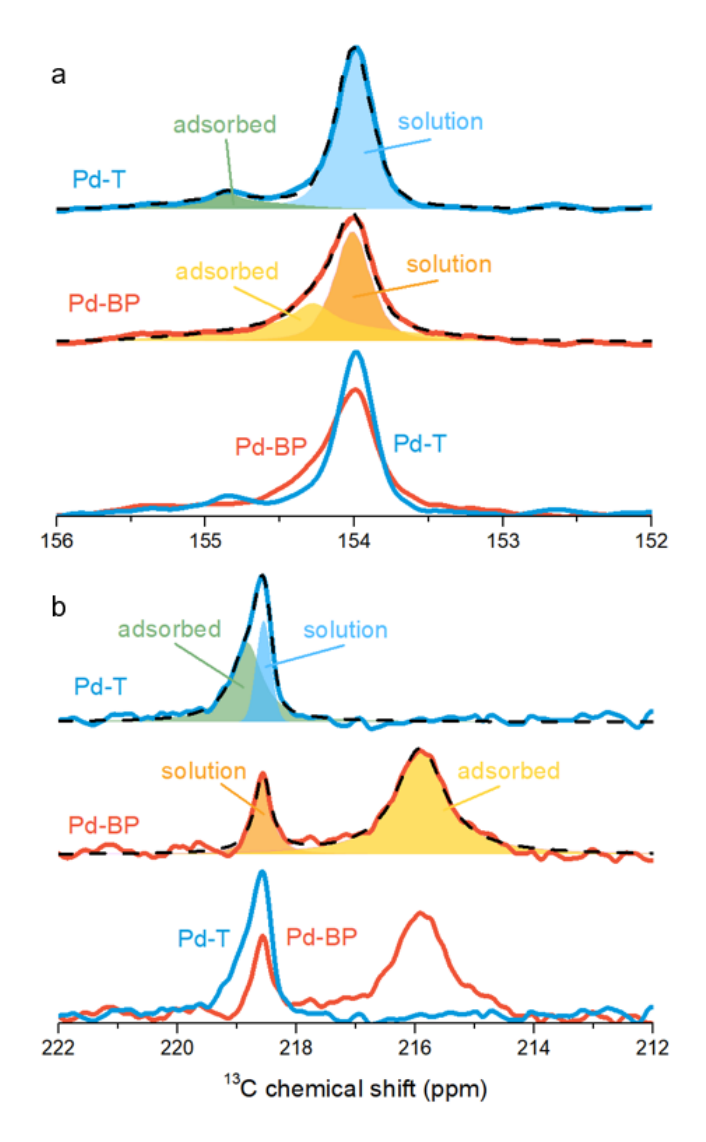


Figure 4. Operando ^{13}C MAS-NMR spectra (solid lines) in (a) the phenol region, and (b) the cyclohexanone region, recorded during phenol hydrogenation catalyzed by Pd-T or Pd-BP. In both experiments, the phenol conversion was ca. 50 %. Shaded areas and dashed lines show the deconvolution results; the data are overlayed in the lowest plot. Each MAS rotor was charged with phenol (64 µmol), catalyst (12 mg, 18 % Pd dispersion, 0.18 µmol surface Pd), water (120 µL), and H_2 (50 bar, 900 µmol), then heated to 75 °C. The pressure increases to ca. 60 bar at the reaction temperature.

Table 3. Analysis of operando ¹³C MAS-NMR spectra recorded during phenol hydrogenation^a

Phase	Catalyst	Phenol		
		δ / ppm	FWHM / Hz	Frac. Area
solution	Pd-T	154.0	0.29	0.85
	Pd-BP	154.0	0.27	0.55
adsorbed		154.8	0.44	0.15

	Pd-BP	154.3	0.49	0.45
		Cyclohexanone		
		δ / ppm	FWHM / Hz	Frac. Area
solution	Pd-T	218.5	0.27	0.43
	Pd-BP	218.5	0.31	0.24
adsorbed		218.8	0.44	0.57
	Pd-BP	216.0	0.99	0.76

^a Reaction conditions as in **Figure 4**.

The 13 C NMR peak for aqueous cyclohexanone appears at 218.5 ppm, with a linewidth (FWHM) of ca. 0.30 Hz, **Figure 4b**. At 50 % phenol conversion in hydrophilic Pd-T, the signal has a downfield shoulder at 218.8 ppm (FWHM = 0.44 Hz) representing adsorbed cyclohexanone (57 %). As predicted, the fraction adsorbed on hydrophobic Pd-BP is higher (76 %), and the FWHM is larger (0.99 Hz). Even more interesting, the peak for adsorbed cyclohexanone is shifted strongly *upfield*, to 216.0 ppm. Ketones show similar behavior in less polar solvents [31–33].

The *ex situ* and *operando* experiments described above show that adsorption of phenol and cyclohexanone is strongly enhanced on Pd-BP, relative to Pd-T. The increased driving force may be enthalpic (stronger interactions with the hydrophobic BP surface compared to the hydrophilic T surface), or entropic (increased degrees of freedom upon adsorption onto BP relative to T), or both. Since the surface hydroxyl densities are very similar for both materials (**Table S1**), a difference in hydrogen-bonding interactions is not a viable explanation. Phenol and cyclohexanone may interact with the aromatic framework linkers of the BP support (e.g., π -stacking interactions in phenol dimers are \sim 4-5 kcal/mol [34]). Entropy may also contribute to the increased driving force for adsorption on BP. Much slower water dynamics at the water-surface interface for BP relative to T was interpreted in terms of water molecule ordering around the nanoscale biphenylene framework linkers [22]. This conclusion was supported by molecular dynamics simulations, which predicted increased tetrahedral ordering of water near the organosilica surface, relative to the inorganic silica surface. Adsorption of an organic solute could liberate this ordered water.

Note that these sorption experiments measure total phenol sorption, including phenol adsorbed on both Pd active sites and the support. In contrast, the kinetically-derived parameters K_{PhOH} and θ_{PhOH} described in the section 3.3 refer only to adsorption on the active sites. However, increased adsorption on the BP support relative to the T support could promote migration of adsorbed molecules to the Pd active sites. The "local" concentrations of phenol and cyclohexanone near the Pd active sites reflects both the concentrations in the pore solution (initially, similar for both catalysts) and the amounts adsorbed on the pore walls. The higher amounts of adsorbed phenol and cyclohexanone on the Pd-BP pore walls relative to Pd-T results in higher coverage of the Pd active sites for Pd-BP (**Figure 3**) and kinetic behavior that is closer to zeroth-order (**Figure 2a**).

These findings also explain the enhanced cyclohexanone selectivity of Pd-BP (**Figure 2b**) despite the similarity in its rate constants ($k_{PhOH} = k_{CyO}$). The *operando* NMR experiments indicate that Pd-BP adsorbs 3× more phenol, but only 1.3× more cyclohexanone, relative to Pd-T (**Table 3**). Therefore, the "local" phenol/cyclohexanone ratio is higher for Pd-BP. Once phenol is fully converted, Pd-BP hydrogenates cyclohexanone faster than Pd-T (**Figure 2b**) because the local

cyclohexanone concentration near the active sites is higher for Pd-BP than for Pd-T (**Table 3**). This explanation assumes that phenol outcompetes cyclohexanone for the active sites even though both phenol and cyclohexanone adsorb strongly to BP. Indeed, a previous study using density functional theory calculations predicted a much higher driving force for phenol adsorption on Pd(111) compared to cyclohexanone [35].

4. Conclusions

In summary, hydrophobic Pd-BP catalyzes phenol hydrogenation faster than hydrophilic Pd-T when other physicochemical characteristics are controlled. The phenol coverage on the active sites is higher for Pd-BP, not because of faster phenol diffusion in the catalyst pores, but because the partitioning of phenol between the aqueous solution and catalyst surface is shifted by the support hydrophobicity. In other words, the increased support hydrophobicity enhances the local concentration of reactants near the active sites, increasing the Pd coverage. The Pd active sites in the hydrophobic BP catalyst are more effectively utilized than in the Pd-T catalyst, where phenol does not fully saturate the active sites. This higher phenol coverage also makes the hydrophobic catalyst more selective to cyclohexanone.

Acknowledgements

HM and CHC gratefully acknowledge funding from the U.S National Science Foundation (NSF), Award No. CHE-1800596, for the catalyst synthesis and experimental NMR measurements. JAC gratefully acknowledges financial support from the U.S. Department of Energy, Office of Science, Division of Basic Energy Sciences, under the Catalysis Science Initiative (DE-FG-02-03ER15467), for the microkinetic modeling. Some experiments made use of the MRL Shared Experimental Facilities, supported by the MRSEC Program of the NSF under Award No. DMR-1720256.

Supplementary Information

The supplementary information is available at the following link: [LINK]

References

- Weber M, Weber M, Kleine-Boymann M (2004) Phenol. In: Wiley-VCH Verlag GmbH & Co. KGaA (ed) Ullmann's Encyclopedia of Industrial Chemistry. Wiley-VCH Verlag GmbH & Co. KGaA, Weinheim, Germany, p a19_299.pub2. DOI: 10.1002/14356007.a19_299.pub2
- 2. Musser MT (2011) Cyclohexanol and Cyclohexanone. In: Wiley-VCH Verlag GmbH & Co. KGaA (ed) Ullmann's Encyclopedia of Industrial Chemistry. Wiley-VCH Verlag GmbH & Co. KGaA, Weinheim, Germany, p a08_217.pub2. DOI: 10.1002/14356007.a08_217.pub2
- 3. Weber M, Pompetzki W, Bonmann R, Weber M (2014) Acetone. In: Wiley-VCH Verlag GmbH & Co. KGaA (ed) Ullmann's Encyclopedia of Industrial Chemistry. Wiley-VCH Verlag GmbH & Co. KGaA, Weinheim, Germany, pp 1–19. DOI: 10.1002/14356007.a01_079.pub4

- 4. Jiang G, Nowakowski DJ, Bridgwater AV (2010) Effect of the Temperature on the Composition of Lignin Pyrolysis Products. Energy Fuels 24:4470–4475. https://doi.org/10.1021/ef100363c
- 5. Zakzeski J, Bruijnincx PCA, Jongerius AL, Weckhuysen BM (2010) The Catalytic Valorization of Lignin for the Production of Renewable Chemicals. Chem Rev 110:3552–3599. https://doi.org/10.1021/cr900354u
- 6. Biesemans B, De Clercq J, Stevens CV, Thybaut JW, Lauwaert J (2022) Recent advances in amine catalyzed aldol condensations. Catal Rev 1–83. https://doi.org/10.1080/01614940.2022.2048570
- 7. Deng Q, Nie G, Pan L, Zou JJ, Zhang X, Wang L (2015) Highly selective self-condensation of cyclic ketones using MOF-encapsulating phosphotungstic acid for renewable high-density fuel. Green Chem 17:4473–4481. https://doi.org/10.1039/C5GC01287B
- 8. Deng Q, Xu J, Han P, Pan L, Wang L, Zhang X, Zou JJ (2016) Efficient synthesis of high-density aviation biofuel via solvent-free aldol condensation of cyclic ketones and furanic aldehydes. Fuel Process Technol 148:361–366. https://doi.org/10.1016/j.fuproc.2016.03.016
- 9. Boot M, Frijters P, Luijten C, Somers B, Baert R, Donkerbroek A, Klein-Douwel RJH Dam N (2009) Cyclic Oxygenates: A New Class of Second-Generation Biofuels for Diesel Engines? Energy Fuels 23:1808–1817. https://doi.org/10.1021/ef8003637
- Bakhtyari A, Sakhayi A, Moravvej Z, Rahimpour MR (2021) Converting Cyclohexanone to Liquid Fuel-Grade Products: A Characterization and Comparison Study of Hydrotreating Molybdenum Catalysts. Catal Lett 151:3343–3360. https://doi.org/10.1007/s10562-021-03575-y
- 11. Chen H, Sun J (2021) Selective hydrogenation of phenol for cyclohexanone: A review. J Ind and EngChem 94:78–91. https://doi.org/10.1016/j.jiec.2020.11.022
- 12. Makowski P, Demir Cakan R, Antonietti M, Goettmann F, Titirici MM (2008) Selective partial hydrogenation of hydroxy aromatic derivatives with palladium nanoparticles supported on hydrophilic carbon. Chem Commun 8:999-1001. https://doi.org/10.1039/b717928f
- 13. Pérez Y, Fajardo M, Corma A (2011) Highly selective palladium supported catalyst for hydrogenation of phenol in aqueous phase. Catal Commun 12:1071–1074. https://doi.org/10.1016/j.catcom.2011.03.026
- 14. Lin C-J, Huang S-H, Lai N-C, Yang C-M (2015) Efficient Room-Temperature Aqueous-Phase Hydrogenation of Phenol to Cyclohexanone Catalyzed by Pd Nanoparticles Supported on Mesoporous MMT-1 Silica with Unevenly Distributed Functionalities. ACS Catal 5:4121–4129. https://doi.org/10.1021/acscatal.5b00380

- 15. Song Y, Wang H, Gao X, Feng Y, Liang S, Bi J, Lin S, Fu X, Wu L (2017) A Pd/Monolayer Titanate Nanosheet with Surface Synergetic Effects for Precise Synthesis of Cyclohexanones. ACS Catal 7:8664–8674. https://doi.org/10.1021/acscatal.7b03463
- 16. Nelson NC, Manzano JS, Sadow AD, Overbury SH, Slowing II (2015) Selective Hydrogenation of Phenol Catalyzed by Palladium on High-Surface-Area Ceria at Room Temperature and Ambient Pressure. ACS Catal 5:2051–2061. https://doi.org/10.1021/cs502000j
- 17. Cantu DC, Wang Y-G, Yoon Y, Glezakou V-A, Rousseau R, Weber RS (2017) Heterogeneous catalysis in complex, condensed reaction media. Catal Today 289:231–236. https://doi.org/10.1016/j.cattod.2016.08.025
- 18. Moon H, Han S, Scott SL (2020) Tuning molecular adsorption in SBA-15-type periodic mesoporous organosilicas by systematic variation of their surface polarity. Chem Sci 11:3702–3712. https://doi.org/10.1039/D0SC00168F
- 19. Hu JZ, Hu MY, Zhao Z, Xu S, Vjunov A, Shi H, Camaioni DM, Peden CHF, Lercher JA (2015) Sealed rotors for in situ high temperature high pressure MAS NMR. Chem Commun 51:13458–13461. https://doi.org/10.1039/C5CC03910J
- 20. Chamas A, Qi L, Mehta HS, Sears JA, Scott SL, Walter ED, Hoyt DW (2019) High temperature/pressure MAS-NMR for the study of dynamic processes in mixed phase systems. Magn Reson Imaging 56:37–44. https://doi.org/10.1016/j.mri.2018.09.026
- 21. Qi L, Chamas A, Jones ZR, Walter ED, Hoyt DW, Washton NM, Scott SL (2019) Unraveling the Dynamic Network in the Reactions of an Alkyl Aryl Ether Catalyzed by Ni/γ-Al₂O₃ in 2-Propanol. J Am Chem Soc 141:17370–17381. https://doi.org/10.1021/jacs.9b09071
- 22. Moon H, Collanton RP, Monroe JI, Casey TM, Shell MS, Han S, Scott SL (2022) Evidence for Entropically Controlled Interfacial Hydration in Mesoporous Organosilicas. J Am Chem Soc 144:1766–1777. https://doi.org/10.1021/jacs.1c11342
- 23. Rice GL, Scott SL (1997) Characterization of Silica-Supported Vanadium(V) Complexes Derived from Molecular Precursors and Their Ligand Exchange Reactions. Langmuir 13:1545–1551. https://doi.org/10.1021/la960679d
- 24. Jelinek L, sz. Kovats E (1994) True Surface Areas from Nitrogen Adsorption Experiments. Langmuir 10:4225–4231. https://doi.org/10.1021/la00023a051
- 25. Walter ED, Qi L, Chamas A, Mehta HS, Sears JA, Scott SL, Hoyt DW (2018) *Operando* MAS NMR Reaction Studies at High Temperatures and Pressures. J Phys Chem C 122:8209–8215. https://doi.org/10.1021/acs.jpcc.7b11442
- 26. Liu Z, Hamad IA, Li Y, Chen Y, Wang S, Jentoft RE, Jentoft FC (2019) Poisoning and competitive adsorption effects during phenol hydrogenation on platinum in water-alcohol mixtures. Appl Catal A: Gen 585:117199. https://doi.org/10.1016/j.apcata.2019.117199

- 27. Li G, Han J, Wang H, Zhu X, Ge Q (2015) Role of Dissociation of Phenol in Its Selective Hydrogenation on Pt(111) and Pd(111). ACS Catal 5:2009–2016. https://doi.org/10.1021/cs501805y
- 28. Zhao D, Feng J, Huo Q, Melosh N, Fredrickson GH, Chmelka BF, Stucky GD (1998) Triblock Copolymer Syntheses of Mesoporous Silica with Periodic 50 to 300 Å Pores. Science 279:548–552. https://doi.org/10.1126/science.279.5350.548
- 29. Lorenc-Grabowska E (2016) Effect of micropore size distribution on phenol adsorption on steam activated carbons. Adsorption 22:599–607. https://doi.org/10.1007/s10450-015-9737-x
- 30. Satterfield CN (1969) Mass Transfer in Heterogeneous Catalysis. The MIT Press, Cambridge.
- 31. Hiraga Y, Chaki S, Niwayama S (2017) ¹³C NMR spectroscopic studies of the behaviors of carbonyl compounds in various solutions. Tetrahedron Lett 58:4677-4681. https://doi.org/10.1016/j.tetlet.2017.10.071
- 32. Kashid SM, Bagchi S (2014) Experimental Determination of the Electrostatic Nature of Carbonyl Hydrogen-Bonding Interactions Using IR-NMR Correlations. J Phys Chem Lett 5:3211–3215. https://doi.org/10.1021/jz501613p
- 33. Faska N, Auhmani A, Esseffar M (2007) Solvent effects on 13C and 1H NMR shielding of cyclic ketones: An experimental and theoretical study. J Mol Struct: Theochemi 811:203–213. https://doi.org/10.1016/j.theochem.2006.12.057
- 34. Živković JM, Stanković IM, Ninković DB, Zarić SD (2020) Phenol and Toluene Stacking Interactions, Including Interactions at Large Horizontal Displacements. Study of Crystal Structures and Calculation of Potential Energy Surfaces. Cryst Growth Des 20:1025–1034. https://doi.org/10.1021/acs.cgd.9b01353
- 35. Zhou H, Han B, Liu T, Zhong X, Zhuang G, Wang J (2017) Selective phenol hydrogenation to cyclohexanone over alkali–metal-promoted Pd/TiO₂ in aqueous media. Green Chem 19:3585–3594. https://doi.org/10.1039/C7GC01318C